6-1998

A V and I CCD Mosaic Survey of the Ursa Minor Dwarf Spheroidal Galaxy

J. T. Kleyna
Harvard-Smithsonian Center for Astrophysics

M. J. Geller
Harvard-Smithsonian Center for Astrophysics

S. J. Kenyon
Harvard-Smithsonian Center for Astrophysics

M. J. Kurtz
Harvard-Smithsonian Center for Astrophysics

J. R. Thorstensen
Dartmouth College

THE ASTRONOMICAL JOURNAL, 115:2359–2368, 1998 June

A V AND I CCD MOSAIC SURVEY OF THE URSA MINOR DWARF SPHEROIDAL GALAXY

J. T. KLEYNA,[1] M. J. GELLER,[1] S. J. KENYON,[1] M. J. KURTZ,[1] AND J. R. THORSTENSEN[2]

Received 1997 October 30; revised 1998 February 17

ABSTRACT

We discuss a Johnson-Cousins V- and I-band CCD mosaic survey of the Ursa Minor dwarf spheroidal galaxy (dSph) to $V \sim 22$. We covered UMi with 27 $10\farcm5 \times 10\farcm5$ overlapping CCD frames, each frame consisting of two 300 s exposures in each of V and I. We also observed several regions $\sim 3°$ from UMi to obtain an estimate of contamination by galaxies and Galactic stars. We report the first H-R diagram of an entire dSph. Separation of dwarf stars from foreground stars by color allows a robust estimation of the structural parameters of UMi. We examine earlier evidence of two lumps in the UMi stellar distribution. We detect a statistically significant asymmetry in the stellar distribution of UMi along the major axis. Structure in the stellar distribution of UMi might indicate a tidal origin for UMi's high observed mass-to-light ratio. We demonstrate a technique for obtaining the absolute magnitude of UMi from horizontal-branch star counts compared with M92; this method of luminosity estimation is independent of the distance to UMi. We obtain $M_V = -8.87 \pm \sigma_{M_V}$, where $\sigma_{M_V} = 0.14$ if M92 is a perfect calibrator and $\sigma_{M_V} \lesssim 0.35$ is an upper bound on the error arising from differences in stellar populations. Our value for M_V is consistent with earlier measurements and has a smaller uncertainty.

Key words: galaxies: dwarf — galaxies: individual (Ursa Minor) — galaxies: stellar content — Local Group

1. INTRODUCTION

The nine dwarf spheroidal (dSph) companions of the Galaxy have been the object of intense scrutiny over recent years. High velocity dispersions, first indicated by observations of Draco (Aaronson 1983), have been interpreted to mean that (1) the dSph's have a very high mass-to-light ratio ($M/L \sim 10^2$ times solar for Ursa Minor and Draco) because of a large dark matter content or (2) they are being tidally disrupted in the Galaxy's gravitational field. Although many investigators favor the dark matter hypothesis (Pryor 1996; Oh, Lin, & Aarseth 1995; Piatek & Pryor 1995), it remains important to examine alternatives with some care.

Various mechanisms have been proposed for the tidal disruption of dSph's. Kuhn & Miller (1989) suggested that a time-dependent Galactic tidal field could pump energy into a dSph by exciting radial oscillations; Sellwood & Pryor (1998), however, find that these modes are not excited by motion through a logarithmic Galactic potential and probably do not account for the high apparent M/L of the dSph's.

Piatek & Pryor (1995) and Oh et al. (1995) performed simulations of dSph tidal disruption and found that the observed velocity dispersion does not rise during disruption; thus the apparent M/L of a dwarf is not significantly inflated by Galactic tides. *Ongoing* tidal disruption is therefore not an explanation of the high apparent M/L of certain dSph's.

Kuhn (1993) argues that dSph's with large apparent M/L may be tidally disrupted remnants that remain coherent because the stars are on similar orbits; Pryor (1996), however, asserts that such disrupted remnants would appear $\gtrsim 10$ times larger than observed dSph's. Kroupa (1997), in a simulation of dwarfs orbiting inside a realistic halo model, finds that it is possible to produce long-lived unbound remnants with many of the properties of the observed dSph's. In particular, Kroupa's remnants have a half-light radius of ~ 200 pc, similar to that of UMi and Draco; Kroupa's remnants also have an inferred $M/L \sim 10^2$ times solar, arising from a favorable line of sight along the orbit. Dispersed remnants may be a viable alternative to a large dark matter content.

Ursa Minor is one of the more interesting dSph's; it has the largest ellipticity (0.55) and, along with Draco, the highest observed velocity dispersion. UMi is a candidate for a disrupted dSph because it is one of the nearest dSph's to the Galaxy.

Several investigators have claimed structure in the stellar number density distribution of UMi on a variety of scales. Olszewski & Aaronson (1985) found small-scale stellar clusters in a limited-area ($\sim 7' \times 10'$) CCD study of UMi to a limiting magnitude of $V = 24.8$. Demers et al. (1995) found a small clump of 78 stars in the center of UMi in a study using two $11' \times 10'$ frames with a limiting apparent magnitude of $R \approx 24$. Irwin & Hatzidimitriou (1995, hereafter IH95), in a study of the whole dwarf from scanned plates, saw a double peak in the stellar surface number density.

In a dynamically stable system with UMi's relatively short crossing timescale $[\sigma_v/(2R_{\rm core}) < 10^8$ yr], structure should be erased. Kuhn (1993) and Kroupa (1997) suggest that the dSph's might be long-lived remnants of tidally disrupted progenitors. Kuhn (1993) notes that there are orbital configurations in which an unbound remnant can survive much longer than the expansion timescale based on the remnant's internal velocity dispersion would suggest. Numerical simulations of disrupted remnants by Kroupa (1997) suggest that the high observed M/L of some dSph's may be explained by an anisotropic velocity distribution combined with a favorable line of sight. Significantly, the remnants in Kroupa's (1997) simulations are not regular, but contain lumps and other forms of structure. The limited number of particles in Kroupa's simulations could,

[1] Harvard-Smithsonian Center for Astrophysics, 60 Garden Street, Cambridge, MA 02138.
[2] Department of Physics and Astronomy, 6127 Wilder Laboratory, Dartmouth College, Hanover, NH 03755-3528.

however, be an issue in comparing the simulations with observed systems.

Here we discuss a V and I CCD survey of UMi, covering an ellipse approximately $60' \times 30'$. Previous surveys of dSph's have been limited to large-area coverage with photographic plates (e.g., Hodge 1964; IH95; Demers, Irwin, & Kunkel 1994), or to smaller regions using a CCD (e.g., Olszewski & Aaronson 1985; Smecker-Hane et al. 1994; Mateo et al. 1991). This paper is the first study that combines the broad areal coverage typical of earlier photographic plates with the photometric depth and accuracy of CCD imaging.

In § 2, we describe the observations and data reduction; in § 3, we describe functional fits to the stellar distribution of UMi. In §§ 4 and 5, we discuss the statistical significance of structure in UMi. In § 6, we estimate the total luminosity of UMi based on horizontal-branch star counts, compared with the globular cluster M92 for calibration. Finally, in § 7 we use horizontal-branch magnitudes to place a limit on the angle our line of sight makes with the major axis of UMi.

2. OBSERVATIONS

We acquired data at the F. L. Whipple Observatory (FLWO) 1.2 m telescope during nine nights. The mosaic survey of UMi consists of a total of 27 fields in Johnson-Cousins V and I. Each field is composed of two 300 s exposures in each of the two filters, and for some fields there are additional 180 s photometric calibration exposures. In addition, we obtained several off-fields 3° from UMi to estimate the background stellar population. We often took V and I exposures of a particular field on different nights to take advantage of moonless periods for the V observations. The field of view is 10.5 on a side, and frames are located on a uniform grid with an overlap of 2.5. The seeing (stellar FWHM) varied from 1.4 to 2.9.

We confirmed photometric nights by examining the rms scatter of standard stars (Landolt 1992) about a linear fit containing the actual magnitude, an air-mass term, and a single $V-I$ color term. Five nights were photometric in V, with an rms scatter of less than 0.015 mag, and two nights were photometric in I, with rms scatters of 0.02 and 0.01 mag, respectively. On the worst of the nonphotometric nights, we measured an extinction of $\lesssim 0.1$ mag. We calibrated out this extinction using overlapping data from photometric nights. Thus, all the data are on a photometric footing. The uncertainties in the V and I magnitude offsets are formally ~ 0.015 mag. The principal source of systematic errors in the photometry is night-to-night variation in the color terms: because V and I data were taken on different nights, and because we could not determine the color terms on nonphotometric nights, we resorted to using average color terms for the entire run. This procedure introduces systematic errors of $\lesssim 0.03$ mag. Figure 1 shows the instrumental V and I histograms for recovered objects, including both stars and galaxies.

We used the recently developed SExtractor package (Bertin & Arnouts 1996) for object identification and photometry. We did not use point-spread function (PSF) fitting photometry, because the PSF varies across the field of view of the FLWO 1.2 m telescope. Also, we did not use the star/galaxy discrimination feature of SExtractor, because it breaks down at the faint magnitudes relevant for most of UMi's stellar population. Instead, we separated UMi objects from background objects by color.

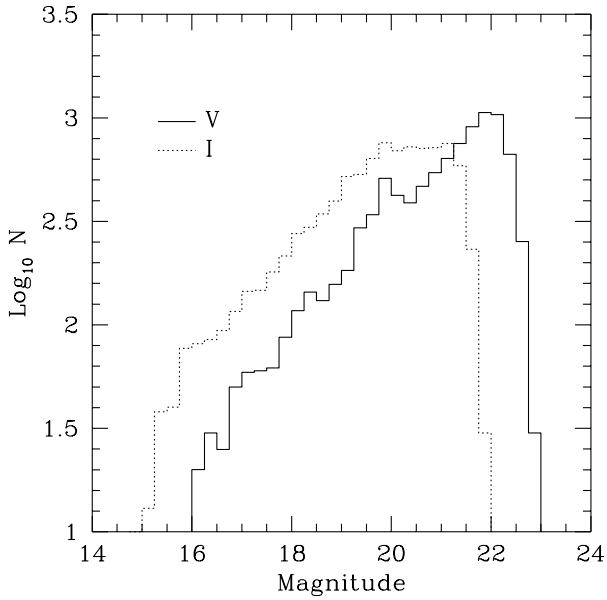

FIG. 1.—Instrumental (not color-corrected) luminosity function for all objects in the survey region. The horizontal branch is visible as the small peak at $V \sim 20$.

SExtractor performs several types of photometry; we used SExtractor's MAG_BEST magnitudes, calculated using an automatically adjusted aperture. Because SExtractor is a relatively new package, we compared MAG_BEST with IRAF DAOPHOT.APPHOT.PHOT aperture magnitudes for two overlapping frames, A and B. We define a set of rms scatters to compare magnitudes for the same objects measured using SExtractor and PHOT for frames A and B; for example, $\sigma_{20}(V_{S,A} - V_{P,B})$ is the rms difference of the SExtractor frame A magnitudes and PHOT frame B magnitudes for all stars brighter than $V = 20$. We find that (1) $\sigma_{20}(V_{S,A} - V_{S,B}) \approx \sigma_{20}(V_{P,A} - V_{P,B}) \approx 0.04$, so that SExtractor is as consistent between frames as PHOT, and (2) $\sigma_{20}(V_{S,A} - V_{P,A}) \approx \sigma_{20}(V_{S,B} - V_{P,B}) \approx 0.04$, so that SExtractor magnitudes agree with PHOT magnitudes within a given frame. We conclude that SExtractor MAG_BEST magnitudes are as accurate as the standard IRAF aperture photometry package. Kleyna et al. (1998) contains the detailed tests.

In addition, we convolved frame A with a Gaussian to double the PSF FWHM. The SExtractor MAG_BEST magnitudes change by an average of 0.016 mag, whereas IRAF PHOT magnitudes change by 0.07 mag. We conclude that SExtractor performs accurate photometry even under conditions of varying seeing. In fact, the magnitudes are more robust than those derived from IRAF.

We determined the global coordinate system (α and δ) of each frame using positions from the US Naval Observatory UJ1.0 Catalog (Monet, Canzian, & Henden 1994). We matched objects by placing them onto a global tangent projection and identifying objects within 1.5 of each other; the final rms deviation in the positions of matched objects is 0.3. To determine whether we double-counted slightly misregistered stars, we examined a histogram of pairwise distances between objects; there is no evidence of an excess of small object separations indicating misregistration.

In regions where frames overlap, the matched list of objects contains a significant bias near the magnitude limit of the survey, because the detection of a faint object is prob-

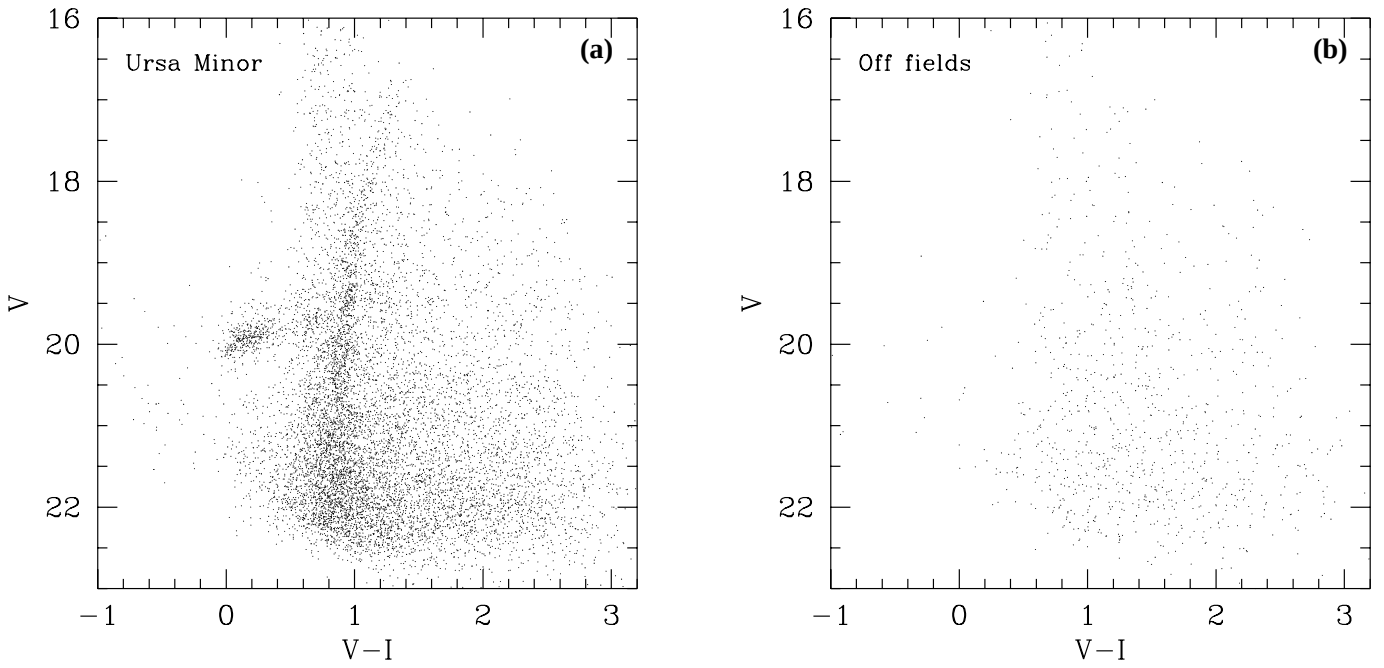

FIG. 2.—(V, $V-I$) CMD of matched objects in (*a*) the survey region and (*b*) off-fields. The giant branch and horizontal branch of UMi are clearly visible in (*a*).

abilistic and an object can be detected several times in an overlap region. To eliminate this bias, we divide our survey region into a grid of 30″ × 30″ squares and associate two V frames and two I frames with each square. To detect an object in a particular grid, we must find it in at least one of these two frames. Thus an object has exactly two chances of detection in each color, even if it lies in a region where many frames overlap. Failure to adopt this uniform procedure introduces detectable spurious structure by producing an artificial stellar number count enhancement at frame edges and corners. Also, SExtractor does not identify objects within an arcminute of extremely bright, saturated stars; to avoid spatial gaps in the data, we filled in these areas with objects copied from a nearby region of comparable area.

Figure 2*a* shows the (V, $V-I$) color-magnitude diagram (CMD) of the UMi data, and Figure 2*b* shows the data for the off-fields. The horizontal and giant branches are clearly visible in the UMi data. In Figure 3, we divide the UMi data into a region approximately corresponding to the horizontal and giant branches of UMi, and a region outside of UMi. We further divide the region inside UMi into (1) shallow and complete data and (2) deep data that extend to the survey's limiting magnitude.

The relative number of stars in the shallow set detected in both V frames, compared with the number detected in only one V frame, implies that the shallow data set is over 99% complete. The deep data set, although it contains more stars, may be subject to systematic effects arising from variations in observing conditions from night to night. The deep data include 3413 objects, the shallow data include 2265 objects, and the outside (non-UMi) data set contains 3611 objects. Separation of objects by color allows us to remove most background objects and to obtain a cleaner determination of the structural parameters of UMi than previously possible.

Consistent with the findings of IH95 and earlier work by Olszewski & Aaronson (1985), the isopleths of the deep UMi data appear to have a secondary maximum or shoulder along the major axis (Fig. 4*b*). Furthermore, the stellar number density falls off more rapidly on the southwest side of UMi than on the northeast side. These features are also visible in the shallow data set (Fig. 4*a*), and are absent in the "outside" data set (Fig. 4*c*), suggesting that they do not arise from observational biases. The features persist when

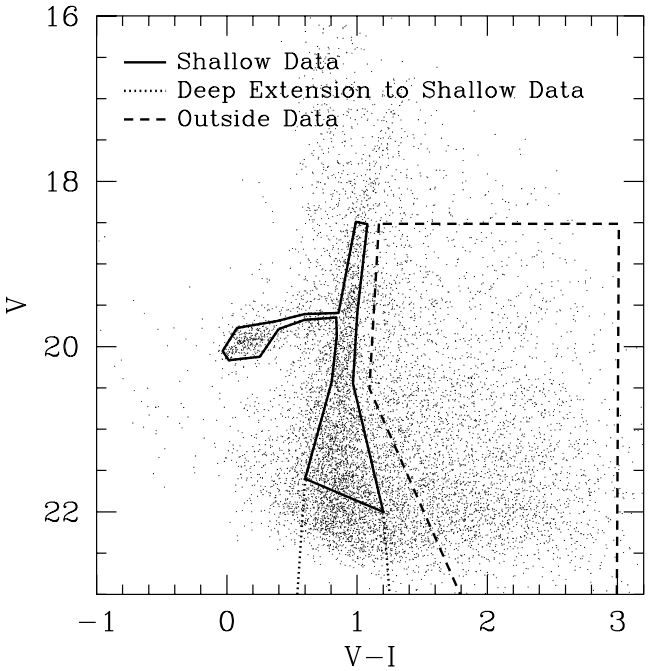

FIG. 3.—(V, $V-I$) CMD of matched objects in the survey region. The shallow and deep regions represent the parts of the survey containing the majority of the UMi stars, and the "outside" data consist principally of Galactic foreground stars and galaxies.

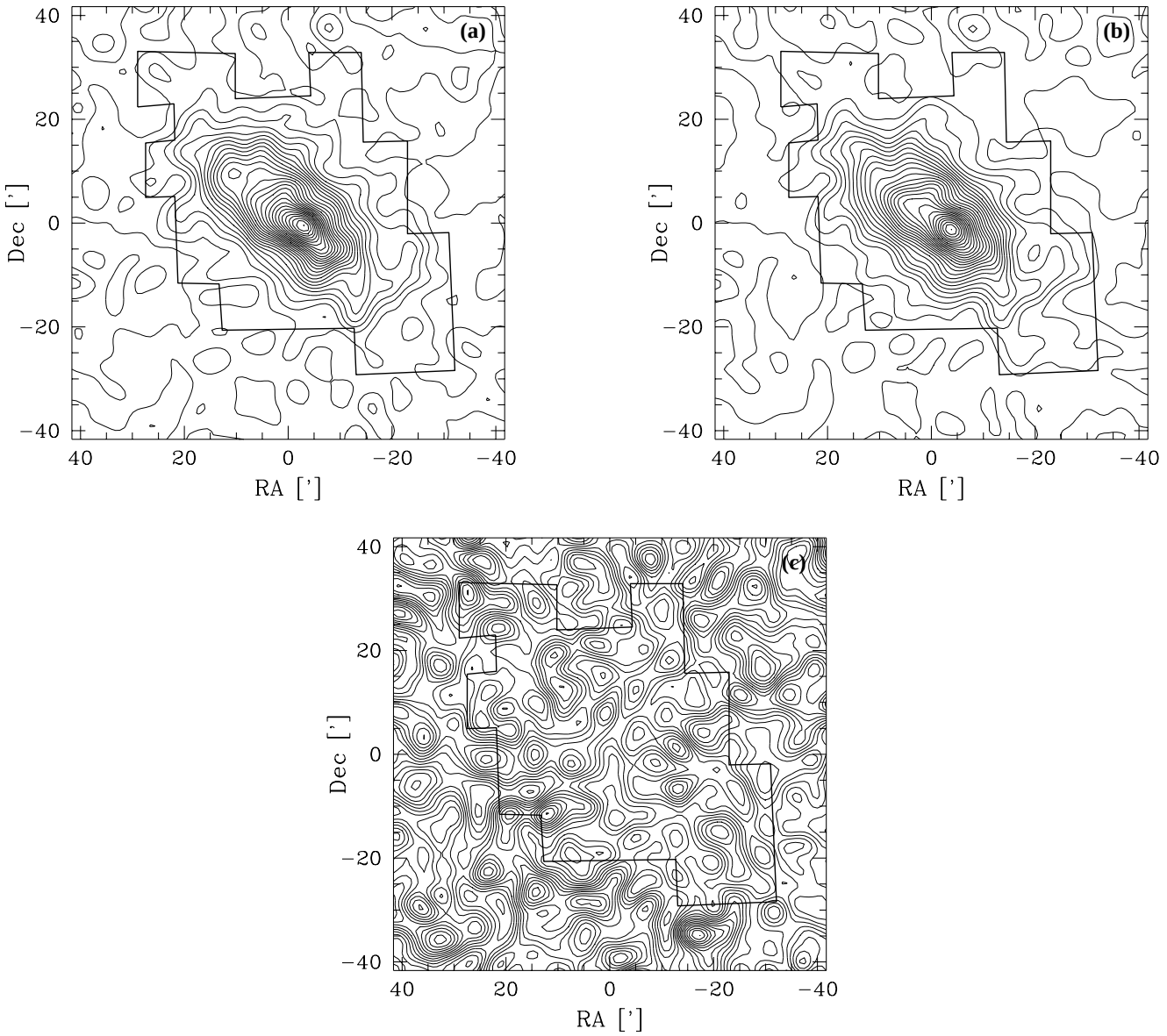

FIG. 4.—Stellar isopleths of UMi after filtering with a 115″ Gaussian kernel: (*a*) and (*b*) (shallow and deep data sets, respectively) show evidence of structure in the form of a secondary lump or shoulder; (*c*) is for the regions of the (V, $V-I$) CMD presumed to be outside of UMi. Contour intervals are 0.14, 0.21, and 0.057 arcmin^{-2} for (*a*)–(*c*). The absence of any features in (*c*) suggests that galaxy clusters do not introduce spurious structure, and that separation of UMi objects from background objects using color was very efficient. The origin of the coordinate system is at $15^{h}08^{m}35\overset{s}{.}8$, 67°24′12″ (B1950.0). The polygon encloses the actual survey region, and we padded the region outside the polygon with a uniform distribution of stars at a density equal to the best-fit background density.

we use only the objects SExtractor identifies as stars. Thus, these features do not result from misidentified clumps of galaxies.

3. FITTING THE STELLAR DISTRIBUTION OF URSA MINOR

Once we eliminate nonmembers of UMi by selecting on color, we use the remaining objects to determine the structural parameters of UMi. Unlike plate-based previous work (e.g., IH95), our photometry is sufficiently good to allow separation of dSph population by color. We thus obtain a more robust and less background-contaminated characterization of the shape of UMi's stellar distribution. For example, our shallow data reach the same central surface density ($\sim$4 arcmin^{-2}) as IH95's ($\sim$4.2 arcmin^{-2}), but our background is approximately 4 times lower because of our selection by color (0.31 arcmin^{-2} vs. 1.16 arcmin^{-2}), which eliminates much of the possible contamination by clusters of galaxies.

To fit the surface number density distribution, we choose a power law with a core (PLC) of the form

$$\Sigma_{\rm PLC}(\boldsymbol{r}) = \frac{M(v-1)}{\pi a^2(1-\epsilon)[1+Q^2(\boldsymbol{r};\,\theta,\,a,\,\epsilon,\,\boldsymbol{r}_0)]^v} + \Sigma_b\,, \quad (1)$$

where M is the total number of stars, Σ_b is the background density, $v > 1$, and Q^2 is a quadratic form in the Cartesian coordinates $\boldsymbol{r} = (x, y)$ such that $Q^2(\boldsymbol{r};\,\theta,\,a,\,\epsilon,\,\boldsymbol{r}_0) = 1$ defines an ellipse centered on $\boldsymbol{r}_0 = (\alpha_0,\,\delta_0)$ with semimajor axis a, semiminor axis $a(1-\epsilon)$, and position angle θ. The value of

Q containing half of the total stars is $Q_{1/2} = (2^{1/(\nu-1)} - 1)^{1/2}$, and the half-mass radius may be defined as $r_{1/2} = a(1-\epsilon)^{1/2}Q_{1/2}$. The $\nu = 2$ case corresponds to a projected Plummer profile, and for $\nu \to \infty$, $\Sigma_{\rm PLC}(r)$ approaches a Gaussian in Q.

We also fit an ellipticized single-component King model (King 1962) of the form

$$\Sigma_{\rm K}(r) = \begin{cases} k\left\{(1+Q^2)^{-1/2} - \left[1 + \dfrac{r_t^2}{a^2(1-\epsilon)}\right]^{-1/2}\right\}^2 + \Sigma_b, \\ \qquad\qquad \text{if } Q^2 \le r_t^2/[a^2(1-\epsilon)], \\ \Sigma_b\,, \qquad\qquad \text{otherwise}, \end{cases} \quad (2)$$

where k is a normalization constant. This model has been widely used to fit dSph's (IH95 and references therein), and it yields a good fit to eight of the known dSph's, albeit with an excess of stars outside the King tidal radius r_t.

To fit a surface number density model $\Sigma(r)$ to a set of observed star positions r_i, we employ a maximum likelihood method. First, we normalize $\Sigma(r)$ to yield $\tilde{\Sigma}(r)$, which has a unit area integral over the survey region; then we maximize the sum $\mathscr{L} = \sum_i \ln \tilde{\Sigma}(r_i)$ over the space of parameters describing the model.

Table 1 lists the best-fit values and errors for both models; we obtain the parameter uncertainties in Table 1 by creating artificial data using the best-fit parameters for the real data and then measuring the scatter of the parameters recovered from these artificial data. Figure 5 overlays the best fits on the observed distribution of stars for the shallow and the deep data.

Though the PLC model produces a slightly better formal fit, the two fitting functions are essentially indistinguishable. The difference between the best-fit $\mathscr{L}$ for the two models is far less than the scatter in $\mathscr{L}$ computed from the artificial data. These data cannot distinguish between the two models.

When we fit the data using a PLC model with the constraint $\nu = 1$ or $\nu = 20$, the fit is considerably worse than either the unconstrained PLC model or the King model. The relatively good fit of the PLC and King models may be a general feature of models with two radial parameters (a and ν for the PLC model, r_c and r_t for the King model) and probably cannot be attributed to any physical suitability of these models. In particular, the extratidal stars previously suggested by King model fits to UMi and other dSph's may, as pointed out by previous authors (IH95), be a measure of the inappropriateness of the King model near its edges rather than an indication of ongoing tidal disruption.

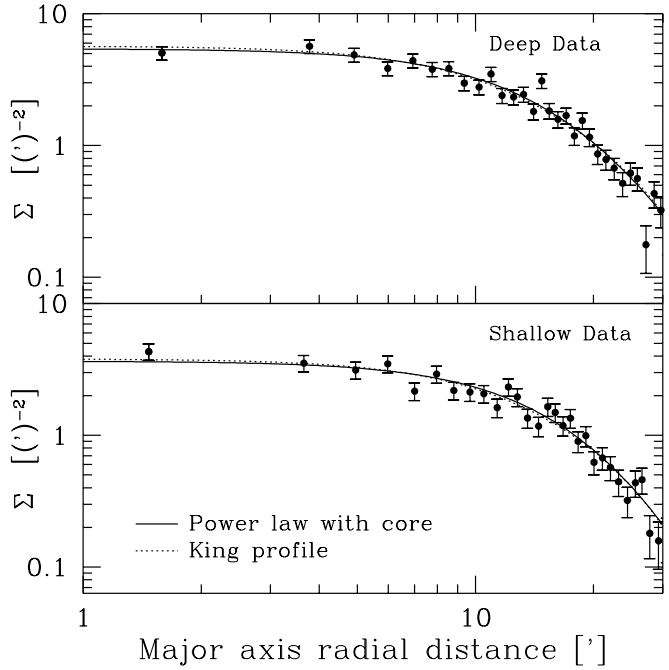

FIG. 5.—Fits of the stellar distribution of UMi to a power-law model with a core (PLC) and to a King model, for the deep and the shallow data. The two models are virtually indistinguishable, although the PLC model yields a slightly better fit for both data sets.

IH95, in their King model fit to UMi, computed best-fit core and tidal radii $r_c = 15\farcm8 \pm 1\farcm2$ and $r_t = 50\farcm6 \pm 3\farcm6$. Our value of r_c (Table 1) agrees well with that of IH95, but our value of r_t is smaller by $\sim$30%. The fit by IH95 extends farther out than ours; their "extratidal" stars may inflate r_t when included in the fit.

To test whether the disagreement between our value of r_t and that of IH95 results from their extratidal stars, we pad our data with a similarly elevated background. We note that the extratidal stars of IH95 are equal to 5%–10% of

TABLE 1

FIT PARAMETERS FOR URSA MINOR

	Shallow Data			Deep Data		
Parameter	Most Likely Value	1 σ Errors	2 σ Errors	Most Likely Value	1 σ Errors	2 σ Errors
PLC model:						
M	1464	$^{+119}_{-89}$	$^{+253}_{-184}$	2273	$^{+168}_{-157}$	$^{+370}_{-256}$
θ (deg)	49.4	$^{+1.6}_{-1.4}$	$^{+2.9}_{-3.1}$	51.0	$^{+1.7}_{-1.3}$	$^{+3.1}_{-2.9}$
α_0 (B1950.0)	15 08 27.5	$\pm 22^{a}$	$^{+40a}_{-41}$	15 08 23.0	$\pm 17^{a}$	$^{+32a}_{-34}$
δ_0 (B1950.0)	+67 25 12	$\pm 20^{a}$	$^{+38a}_{-41}$	+67 24 30	$\pm 17^{a}$	$^{+33a}_{-34}$
a (arcmin)	26.9	$^{+8.8}_{-4.8}$	$^{+58.4}_{-8.0}$	22.4	$^{+5.4}_{-2.8}$	$^{+11.1}_{-5.6}$
ϵ	0.554	$^{+0.023}_{-0.019}$	$^{+0.043}_{-0.044}$	0.519	± 0.020	± 0.040
ν	3.53	$^{+1.85}_{-0.84}$	$^{+22.60}_{-1.37}$	2.80	$^{+0.97}_{-0.46}$	$^{+2.38}_{-0.84}$
r_{50} (arcmin)	10.09	$^{+0.67}_{-0.48}$	$^{+1.44}_{-0.82}$	10.62	$^{+0.73}_{-0.59}$	$^{+1.46}_{-0.94}$
Σ_b (arcmin^{-2})	0.305	$^{+0.024}_{-0.027}$	$^{+0.049}_{-0.046}$	0.461	$^{+0.032}_{-0.031}$	$^{+0.064}_{-0.056}$
King model:						
r_c (arcmin)[b]	15.2	$^{+2.3}_{-2.1}$	$^{+7.0}_{-3.7}$	13.6	± 1.5	$^{+3.1}_{-2.2}$
r_t (arcmin)	34.0	$^{+2.9}_{-2.4}$	$^{+6.5}_{-4.9}$	39.1	$^{+4.3}_{-3.2}$	$^{+9.4}_{-5.6}$

NOTES.—Maximum likelihood fit parameters for Ursa Minor, for deep and shallow data sets. Units of right ascension are hours, minutes, and seconds, and units of declination are degrees, arcminutes, and arcseconds.

[a] Arcseconds.

[b] Where $r_c = a(1-\epsilon)^{1/2}$.

their background density. Hence we pad the region outside our data with a $50' \times 50'$ box of background stars, with a density 10% higher than our off-field background. When we fit a King model to this padded data, our value of r_t increases to that found by IH95.

An important concern is that our limited off-field coverage may affect our ability to estimate the background and may make our other fit parameters less reliable. However, we note the following: (1) Our Monte Carlo estimates of the errors on the fit parameters include uncertainties in the background. (2) Although we know the background to within 0.03 arcmin^{-2}, versus 0.01 arcmin^{-2} for IH95, the $\sqrt{N}$ variations in the higher background of IH95, taken across the face of UMi, eliminate this disadvantage. Taking both the uncertainty and Poisson noise in the background into account, IH95 expect about 900 ± 31 background stars within the core radius of UMi; we expect 240 ± 28. (3) Our background estimates using two off-fields on opposite sides of UMi match at the 0.44 σ level, suggesting that systematic variations in the background are not a problem. Finally, the value of the fit parameters is insensitive to the method we use to determine the background; the result is the same for a background based entirely on the off-fields, or based on both the off-fields and the central survey region.

4. METHOD FOR TESTING THE SIGNIFICANCE OF THE SECONDARY PEAK

Several authors, beginning with Olszewski & Aaronson (1985), have reported structure in the stellar distribution of UMi. Demers et al. (1995) reported a concentration of stars at the center of UMi, but their survey covered only the central region of the dwarf. The photographic plate study of IH95 covers all of UMi to a depth roughly comparable to our shallow data; their Figure 1*h* shows a secondary peak comparable to our Figure 4*a*. However, this peak does not show up in our deeper Figure 4*b*; there is only an extended shoulder in the stellar distribution. Possibly, the secondary maximum seen by IH95 and in our shallow data is a Poisson noise artifact present among the brightest stars of UMi. In fact, when we construct artificial data sets using the parameters of our fits to UMi, these sets often contain features very similar to the secondary peak in the shallow UMi data. Figure 6, for example, shows an artificial realization of our shallow data, created using our best-fit PLC parameters. Although these data were drawn from a smooth distribution, they appear as lumpy as the shallow UMi data set (Fig. 4*a*).

Conventional statistical tests for structure in clusters of objects (see Pinkney et al. 1996 for a comparison) are unsuitable for our study of UMi. For instance, the Lee statistic (Fitchett & Webster 1987) depends on using second moments of projected line densities to find a dispersion-minimizing division of the data; the second moment, however, diverges in the presence of a uniform background and, even in the absence of a background, is divergent for many distributions of astrophysical interest. The path linkage criterion employed by Demers et al. (1995) to find lumps in four dSph's is applicable over regions small enough that the stellar number density is approximately constant; this method is also unsuitable for detecting the relatively large scale structure that may be present in UMi.

We have devised a simple statistic, therefore, to quantify what the human eye perceives as large-scale lumpiness: we divide the data into several equal-size sets, find the location

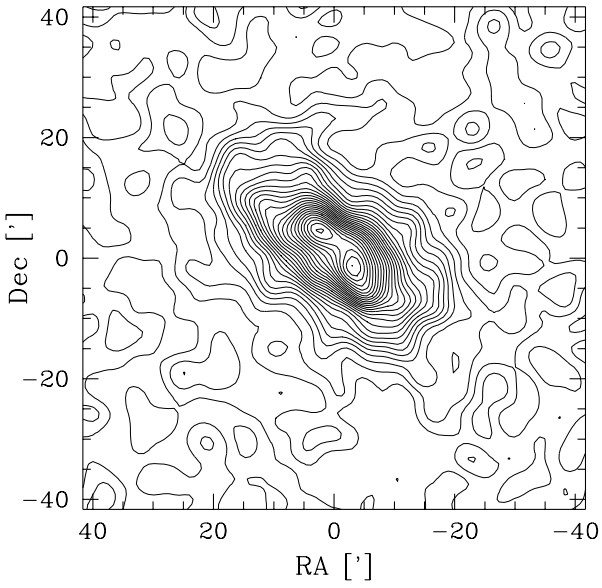

FIG. 6.—Isopleths for artificial data created using the best-fit PLC model for the shallow data, containing the same number of objects as the artificial data set. These data, although drawn from a smooth distribution with a single peak, appear as bimodal as the shallow data set (Fig. 4*a*).

of the second-highest peak in each set, and determine the strength of the correlation of the locations of these secondary peaks among the divisions. We then compare the statistic with Monte Carlo data drawn from a best-fit smooth distribution (§ 3) to test whether the actual distribution is lumpier than the artificial data.

The exact procedure is as follows:

1. For each of N_s random shuffles of a set of stars S, divide the shuffled data into N_g subgroups s_{ij}, where $i = 1, \ldots, N_s$ indexes the shuffle and $j = 1, \ldots, N_g$ indexes the subsets within a shuffle.

2. For each s_{ij}, generate a smooth distribution by applying a Gaussian filter to the stellar distribution along a $50''$ grid. On each grid, let $\boldsymbol{r}_{ij}$ denote the position of the second-highest local maximum grid point.

3. For each shuffle i, sum over the secondary peaks to calculate the statistic

$$\alpha_i = -\sum_{j'>j} \ln(|\boldsymbol{r}_{ij} - \boldsymbol{r}_{ij'}|^2 + 1) . \quad (3)$$

We obtain the form of this statistic by noting that the probability that two points in a two-dimensional uniform distribution fall within a distance of r of each other is $\propto r^2$; thus, equation (3) is a crude likelihood equation, with $\alpha_i = 0$ when the secondary maxima are perfectly correlated in the N_g subsamples. The purpose of the 1 inside the parentheses is to keep the statistic bounded if two maxima should fall on the same grid point.

4. Use $\bar{\alpha} = \sum_i \alpha_i / N_g$ as the measure of the strength of a secondary peak of the original set S. A value of α that is close to zero indicates that the distribution contains a strong secondary peak, because the original peak in S persists among the subsamples s_{ij}.

We take this approach because, although it is difficult to characterize the significance of a peak in a smoothed, spatially nonuniform distribution of stars, it is obvious that spurious peaks caused by random noise have a height that scales as the square root of the total number of stars. If the

original distribution, S, contains a 2 σ spurious peak and we divide S into four resamplings s_j, then each s_j has one-fourth of the original peak, which will be at a 1 σ significance within s_j. The remnant of the original peak will thus compete with additional 1 σ peaks introduced by the resampling process, and the original peak in S will be judged insignificant. If the original peak in S were more significant (e.g., 4 σ), then the spurious peaks introduced by the resampling would not drown out the remnants of the original peak in the s_j as often. A significant detection would result because the remnant peaks in the s_j would be correlated.

Essentially, each resampling s_j introduces additional random noise and spurious peaks on top of any peaks in the original distribution S. A value of $\bar{\alpha}$ close to zero indicates that an original peak in S dominates the random peaks introduced in the resampling process.

We obtain the significance of $\bar{\alpha}$ by applying our technique to random data drawn from a PLC distribution. We ask whether the $\bar{\alpha}$ of the observed data set is significantly larger than that for the simulated data. We obtain the PLC parameters used to construct the null hypothesis by first generating distributions based on the best-fit parameters for the real data; we then recover the parameters using the maximum likelihood approach in § 3. This two-stage approach incorporates the errors in the best-fit parameters into the final measure of significance and tends to decrease the significance of the $\bar{\alpha}$ in the real data.

In tests using artificial data, the $\bar{\alpha}$-statistic is sensitive enough to detect a $\sim$75-star 140″ Gaussian lump in a data set with the same number of stars as our shallow data. Other tests, including the Lee statistic (Fitchett & Webster 1987), do not recover such lumps. Like many tests, our method has the disadvantage of requiring a parametric fit to construct the null hypothesis; it has the further disadvantage of being dependent on a smoothing scale.

The observed features in the isopleths of UMi are dominated by random noise at a Gaussian smoothing scale of $\lesssim$100″ and are smoothed out entirely at a smoothing scale $\gtrsim$200″; hence we limit our search for significant lumpiness to four filter values between these extremes. In the shallow data, we do not detect a significant secondary maximum in the stellar surface number density; in the deep data, we obtain a significant detection only at a 115″ smoothing scale, and the detection is only at the $p = 0.05$ level. The low significance of the statistic, further weakened by the filter-scale tuning required to obtain a detection, makes the attempt to detect a secondary peak in UMi inconclusive.

Figure 7 shows the positions of the primary and secondary peaks for each resampling s_{ij} of the deep data set. It is apparent that the location of the secondary peak disagrees with the secondary peak in our Figure 4*a* and in Figure 1*h* of IH95. It does, however, correspond to the shoulder on the northeast side of the major axis in Figure 4*b*. A plot of lump positions for the shallow data, analogous to Figure 7, shows that the second peak of the resamplings s_{ij} is not concentrated in one place. We conclude that the secondary peak we see in Figure 4*a* is an artifact of small number statistics. The shoulder in Figure 4*b*, however, is probably a real feature of the data. Because Olszewski & Aaronson (1985), using deeper data covering 6′ × 10′, claim evidence of a secondary peak, the possibility of a bimodal distribution cannot be dismissed without deeper data covering the entire dwarf.

5. ASYMMETRY

The surface number density contour diagram of UMi (Fig. 4) is apparently asymmetric; the isopleths are more closely spaced on the southwest side of the major axis than on the northeast side. We know of no mechanism for sustaining such an asymmetry in an equilibrium dynamical system.

To rule out the possibility that the stellar distribution is actually symmetric, and that the observed asymmetry arises from Poisson noise, we construct a simple asymmetry statistic, β (Fig. 8). First, we filter the distribution along the

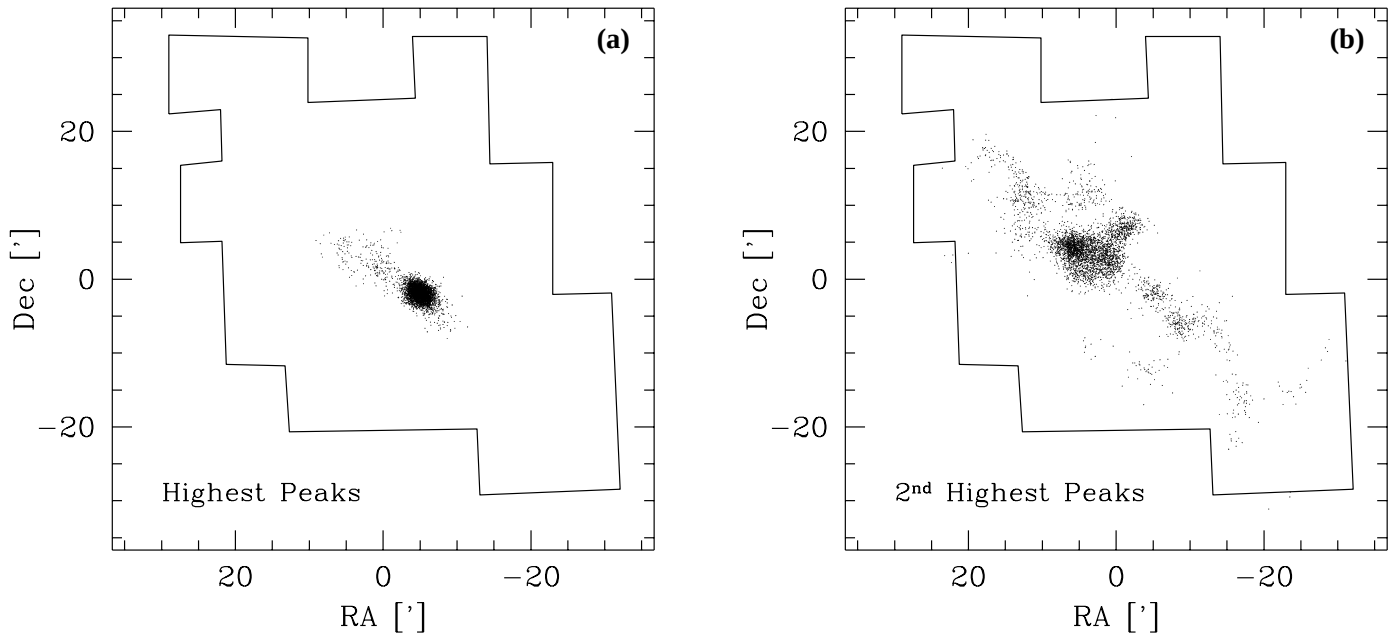

FIG. 7.—Locations of highest and second-highest peaks in the deep data set. Each point comes from a single resampling s_{ij} (§ 4). The location of the secondary maximum is closer to the center of UMi than in previous studies (IH95), and the significance of the detection of the second peak is only 2 σ.

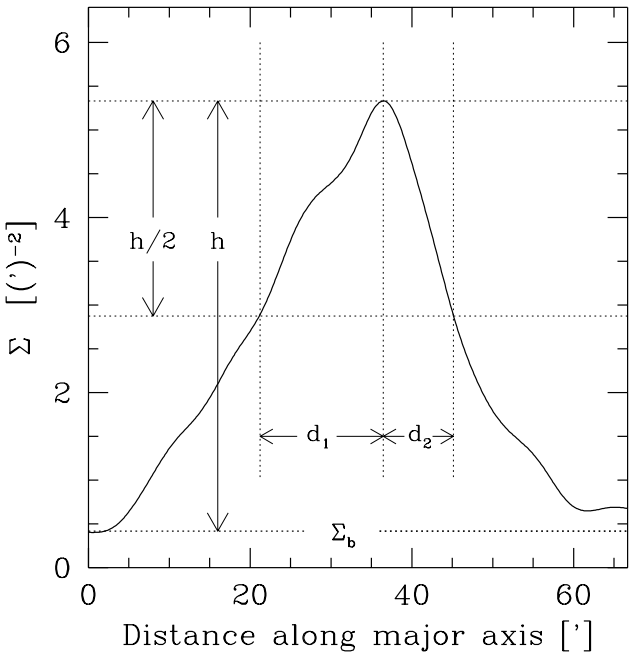

FIG. 8.—Asymmetry statistic, where h is the maximum background-subtracted stellar surface number density along a line down the major axis; d_1 and d_2 (with $d_1 \geq d_2$) are the distances at which the density falls to $h/2$, and the asymmetry statistic is given by $\beta = d_1/d_2 - 1$. The density curve shown is for the deep data set, with a 150″ Gaussian filter; for this curve, $\beta = 0.7$. Distance increases from northeast to southwest.

major axis with a two-dimensional Gaussian. Next, we let d_1 and d_2 be the distances where the filtered distribution falls to half its maximum value, requiring that $d_1 \geq d_2$. Finally, we define the asymmetry as $\beta = d_1/d_2 - 1$. To test the significance of the observed β, we calculate β for 1000 simulated distributions using the best-fit PLC models (a similar procedure to the significance computation for the $\bar{\alpha}$-statistic). Table 2 shows β for the deep and shallow data for two Gaussian filter widths. We also compare the value of β for the shallow data set with the β for simulated deep data sets to allow for systematic effects. Except for the shallow data with a 150″ filter, the actual data are asymmetric at a greater than $2\,\sigma$ ($p < 0.05$) significance level, with the 250″ deep data significant at the $\sim 3\,\sigma$ ($p \sim 0.003$) level.

The deep data are consistently more asymmetric than the shallow data. An observational bias, such as a brighter detection threshold on the southwest (steeper) side of the major axis, would produce this difference. If we assume a worst-case 0.1 mag difference in limiting depth, consistent with the maximum night-to-night excursions of the photometric solutions, and if we approximate the V luminosity function of Figure 1 as the power law $N(m) \propto 10^{0.3m}$, then we underestimate the surface number density on the southwest side of the major axis by a relative factor of 1.08 compared with the northeast side. The inclusion of this rescaling factor decreases the significance of the asymmetry of the deep data to the $p = 0.02$ level and makes the value of β for the deep data equal to that for the shallow data. However, the difference between the *mean* extinction for the southwest and northeast sides of the major axis is actually only 0.01 mag; hence, the significance of the asymmetry is greater in the deeper data.

As another test of asymmetry, we project stars in a 10′-wide band around the major axis onto the major axis and perform a Kolmogorov-Smirnov (K-S) comparison between the northeast and southwest sides of the projected distribution; the point on the line where the distribution is split is selected to minimize the significance of the asymmetry. This K-S test shows that the shallow (deep) data are asymmetric at the $p = 0.2$ ($p = 0.01$) significance level.

TABLE 2

ASYMMETRY STATISTIC β

Data Set	Filter Width (σ) (arcsec)	β	Significance
Shallow.....	150	1.50	0.18
Shallow.....	250	1.36	0.06
Deep.....	150	1.76	0.035
Deep.....	250	1.46	$\lesssim$0.001
Mixed	250	1.36	0.01

NOTES.—Asymmetry statistic β and significance for deep and shallow data at two Gaussian filter widths. "Mixed" data compare the value $\beta = 1.36$ obtained for the shallow data set with the β obtained for artificial data with the same number of stars as the deep data set.

6. LUMINOSITY ESTIMATE FOR URSA MINOR

Much of the difficulty in deriving the mass-to-light ratio of UMi arises from the large uncertainty in the luminosity. It is difficult to estimate UMi's total luminosity by integrating the observed luminosity function directly, because (1) our catalog of UMi's population is contaminated with a large number of galaxies and Galactic stars, (2) our small number of off-fields makes it difficult to remove this contamination, and (3) our survey does not reach the main-sequence turnoff.

However, Olszewski & Aaronson (1985) found that the age and metallicity of UMi's stellar population are very similar to those of the globular cluster M92. Therefore, if we take the claim of Olszewski & Aaronson (1985) at face value, we can estimate the luminosity of UMi by assuming that the fraction of the total luminosity contributed by the blue horizontal branch (HB) is the same for UMi and M92. Then we can measure the luminosity of UMi by rescaling the luminosity of M92 by the relative HB star counts. Our estimate of $M_{V,\mathrm{UMi}}$, the absolute V magnitude of UMi, is completely independent of the distance to UMi.

The total number of HB stars in our survey region is 368 ± 36; the uncertainty is only 10% because there is little contamination in the region of the color-magnitude diagram corresponding to the HB. Using data provided by M. Bolte (1997, private communication), we count 300 ± 17 stars in the HB of M92, implying that $L_{\mathrm{UMi}}/L_{\mathrm{M92}} = 1.33 \pm 0.13$, or $M_{\mathrm{UMi}} - M_{\mathrm{M92}} = -0.31 \pm 0.10$.

The apparent luminosity of M92 is $V = 6.39 \pm (\lesssim 0.05)$, with a V-band extinction of 0.065 mag (Webbink 1985). The distance modulus of M92 is less certain, however. Reid (1997), using *Hipparcos*-recalibrated subdwarf fitting, obtains $(m - M)_{\mathrm{M92}} = 14.93 \pm 0.1$. Storm, Carney, & Latham (1994), using the completely independent Baade-Wesselink method, obtained $(m - M)_{\mathrm{M92}} = 14.60 \pm 0.26$. These results are consistent at the 0.24 significance level; we combine them to obtain $(m - M)_{\mathrm{M92}} = 14.89 \pm 0.09$. Furthermore, Caloi, D'Antona, & Mazzitelli (1997) compute $(m - M)_{\mathrm{M92}} = 14.72$ using HB modeling; they did not report an error. If we estimate their uncertainty as 0.2 mag, the results of Caloi et al. (1997) are consistent with the other

distance moduli at the 0.43 significance level, changing our value for $(m - M)_{M92}$ by only 0.03 mag.

Combining the apparent luminosity of M92 with its distance modulus, we obtain an absolute luminosity $M_{V,M92} = -8.57 \pm 0.09$; this value is almost 0.4 mag brighter than the commonly tabulated value, but it is consistent with Reid's (1997) finding that the distance to M92 has historically been underestimated. Combining $M_{V,M92}$ with the relative HB star counts yields $M_{V,UMi} = -8.87 \pm 0.14$. This value is consistent with previous estimates (-8.7, Webbink 1985; -8.9, Caldwell et al. 1992; -8.5 ± 0.5, IH95). Our error on $M_{V,UMi}$ assumes that M92 is a perfect calibrator, and that the only important contribution to the uncertainty is from the distance modulus of M92.

We can also apply the HB star count method to estimate the known luminosity of M5 from the data of Sandquist et al. (1996) based on M92. The result differs from the observed absolute magnitude of M5 by 0.35 mag. This disagreement implies that differences in stellar populations between M5 and M92 lead to an additional ~ 0.32 mag error term, after removing the contribution from error in the distance moduli. Because the metallicity of M5 is higher than that of M92 and UMi ($[Fe/H]_{M5} \approx -1.3$ vs. $[Fe/H]_{M92,UMi} \approx -2.1$), the 0.32 mag error is probably an upper limit.

Our measurement of $M_{V,UMi}$ does not account for variations in stellar populations, because we compare UMi only with M92. For example, the horizontal branch of UMi spans a range in V magnitude about 0.2 mag smaller than the range of the horizontal branch of M92, an effect that Olszewski & Aaronson (1985) probably did not notice because of their small survey area. A comparison of several low-luminosity globular clusters would lead to a better estimate of the error.

Upon rescaling the mass-to-light ratio from Table 10 of IH95, our value of $M_{V,UMi}$ reduces the mass-to-light ratio of UMi from $(M/L)_{UMi} = 90 \pm 43$ to 70^{+30}_{-20} times solar, where the error is based on the conservative 0.35 mag error estimate on $M_{V,UMi}$.

7. PROJECTION EFFECTS

One of Kroupa's (1997) two disrupted remnant simulations has a large apparent M/L through a favorable (17°.5) line-of-sight alignment of the model dwarf's orbit. In this model, an observer interprets projected tidal streaming as a large velocity dispersion. To test whether the long axis of UMi is being viewed in projection, we divide UMi's HB into two sets along the major axis; the first set consists of all stars at least 10′ to the northeast of the center, and the second set consists of all stars at least 10′ to the southwest. If we are viewing the major axis in projection, we expect a difference in the mean magnitudes of the two sets.

Taking the distance to UMi, $D_{UMi} = 65$ kpc, and the major-axis core radius, $r_c \approx 200$ pc, we expect a magnitude difference of $\Delta M \approx 5 \log [1 + 2r_c/(D_{UMi} \tan 17°.5)] \approx 0.04$. For our southwest and northeast HB star sets, we obtain mean magnitude differences $\langle V \rangle_{SW} - \langle V \rangle_{NE} = 0.025 \pm 0.021$ and $\langle I \rangle_{SW} - \langle I \rangle_{NE} = 0.036 \pm 0.035$. The uncertainties in these values come principally from the intrinsic spread of the horizontal branch.

The differences in magnitude we observe are consistent at the 1 σ level both with projection angles ranging from 90° (no projection) to less than 17°.5. It is suggestive, however, that the results for V and I agree in sign and size; thus, a favorable projection angle cannot be ruled out.

8. CONCLUSION

Olszewski & Aaronson (1985), Demers et al. (1995), and IH95 have reported structure in the Ursa Minor dSph on various scales. The presence of structure is important because it suggests that tidal disruption may play a role in the large apparent M/L of UMi and other dSph's.

We have examined the evidence for structure by performing a large-scale V- and I-band CCD survey of UMi and constructing the first CCD H-R diagram of a complete dSph. Because we have good-quality two-color photometry, we are able to remove much of the foreground star and background galaxy contamination from our catalog of UMi stars, giving a more robust estimate of UMi's structural parameters.

The isopleth plot of our shallow data (Fig. 4*a*) shows the secondary peak in the surface stellar number density reported earlier by IH95, but it vanishes in our deeper data set. Using a resampling technique, we demonstrate that the secondary peak is statistically insignificant in the shallow data. In the deeper data set, the shoulder in the isopleth map (Fig. 4*b*) corresponds to a secondary peak that is significant at the $\lesssim 2\ \sigma$ level.

Several asymmetry statistics show that the shallow data are asymmetric along the major axis at the $\lesssim 2\ \sigma$ level and the deep data are asymmetric at the 3 σ level. Because of the steep power-law shape of the luminosity function (Fig. 1), however, the deep data are subject to unknown systematic biases, which might reduce the asymmetry in the deep data to the 2 σ level.

We also use the H-R diagram to obtain an improved estimate of UMi's luminosity. Under the assumption that UMi and the globular cluster M92 have similar stellar populations, we used the ratio of the number of HB stars in UMi and M92 to compute UMi's luminosity. Our value of $M_V = -8.87 \pm \sigma_{M_V}$ ($0.14 < \sigma_{M_V} < 0.35$) agrees with brighter previous estimates and implies a mass-to-light ratio of $(M/L)_{UMi} = 70^{+30}_{-20}$ times solar. Our method of measuring the luminosity of UMi is applicable to other dSph's and has the advantage that it is independent of the dSph distance modulus.

Finally, we use the variation of the mean HB magnitude across UMi to place a limit on the angle our line of sight makes with UMi's major axis. Our data are consistent both with an angle of 90° (no projection of the major axis) and with an angle of 17°.5; the latter projection angle was the source of a large apparent M/L in one of the models of Kroupa (1997).

A CCD survey with a wide-field camera to a limiting magnitude of $V \gtrsim 24$ would easily reach the main-sequence turnoff, providing a much large population of stars to study. Because we find statistically significant signs of structure in data with $V \lesssim 23$, deeper data would yield an unambiguous measure of the structure of the dwarf.

We thank Michael Bolte for allowing us to use his globular cluster data and Chris Kochanek for helpful discussions. We also thank the MDM Observatory staff, and the staff of Fred Lawrence Whipple Observatory, for their assistance in obtaining observations. This research was supported by the Smithsonian Institution.

REFERENCES

Aaronson, M. 1983, ApJ, 266, L13
Bertin, E., & Arnouts, S. 1996, A&AS, 117, 393
Caldwell, N., Armandroff, T., Seitzer, P., & Da Costa, G. S. 1992, AJ, 103, 840
Caloi, V., D'Antona, F., & Mazzitelli, I. 1997, A&A, 320, 823
Demers, S., Battinelli, P., Irwin, M. J., & Kunkel, W. E. 1995, MNRAS, 274, 491
Demers, S., Irwin, M. J., & Kunkel, W. E. 1994, AJ, 108, 1648
Fitchett, M., & Webster, R. 1987, ApJ, 317, 653
Hodge, P. W. 1964, AJ, 69, 438
Irwin, M. J., & Hatzidimitriou, D. 1995, MNRAS, 277, 1354 (IH95)
King, I. 1962, AJ, 471, 67
Kleyna, J. T., Geller, M. J., Kenyon, S. J., Kurtz, M. J., & Thorstensen, J. R. 1998, in preparation
Kroupa, P. 1997, NewA, 2, 139
Kuhn, J. R. 1993, ApJ, 409, 13
Kuhn, J. R., & Miller, R. H. 1989, ApJ, 341, L41
Landolt, A. U. 1992, AJ, 104, 340
Mateo, M., Nemec, J., Irwin, M. J., & McMahon, R. 1991, AJ, 101, 892
Monet, D., Canzian, B., & Henden, A. 1994, BAAS, 185, No. 6.01
Oh, K. S., Lin, D. N. C., & Aarseth, S. J. 1995, ApJ, 442, 142
Olszewski, W. W., & Aaronson, M. 1985, AJ, 90, 2221
Piatek, S., & Pryor, C. 1995, AJ, 109, 1071
Pinkney, J., Roettiger, K., Burns, J. O., & Bird, C. M. 1996, ApJS, 104, 1
Pryor, C. 1996, in ASP Conf. Ser. 92, Formation of the Galactic Halo—Inside and Out, ed. H. L. Morrison & A. Sarajedini (San Francisco: ASP), 424
Reid, I. N. 1997, AJ, 114 161
Sandquist, E. L., Bolte, M., Stetson, P. B., & Jesser, J. E. 1996, ApJ, 470, 910
Sellwood, J. A., & Pryor, C. 1998, Highlights Astron., in press
Smecker-Hane, T. A., Stetson, P. B., Hesser, J. E., & Lehnert, M. D. 1994, AJ, 108, 507
Storm, J., Carney, B. W., & Latham, D. W. 1994, A&A, 290, 443
Webbink, R. F. 1985, in IAU Symp. 113, Dynamics of Star Clusters, ed. J. Goodman & P. Hut (Dordrecht: Reidel), 541